CORE
Metadata, citation and similar papers at core.ac.uk
Provided by Woods Hole Open Access Server

The composition of dissolved iron in the dusty surface ocean: an exploration using size-fractionated iron-binding ligands

Jessica N. Fitzsimmons[*ab], Randelle M. Bundy[c], Sherain N. Al-Subiai[bd], Katherine A. Barbeau[c], Edward A. Boyle[b]

[a] Rutgers University, Marine Biogeochemistry, 71 Dudley Road, New Brunswick, NJ 08901, USA

[b] Massachusetts Institute of Technology/Woods Hole Oceanographic Institution, Chemical Oceanography, 77 Massachusetts Avenue Cambridge, MA 02139, USA

[c] Scripps Institution of Oceanography, University of California San Diego Geosciences Research Division, 9500 Gilman Drive La Jolla, CA 92093, USA

[d]Environment Management Program, Environment and Life Sciences Research Center, Kuwait Institute for Scientific Research, Kuwait

[*]Corresponding author:
Jessica Fitzsimmons
Rutgers University
Institute of Marine and Coastal Science
71 Dudley Road
New Brunswick, NJ 08901
Email: jessfitz@marine.rutgers.edu

ACCEPTED MANUSCRIPT

ACCEPTED MANUSCRIPT

Keywords

iron
iron ligands
CLE-ACSV
colloids
ultrafiltration
trace metals
GEOTRACES
North Atlantic Ocean
chemical oceanography

ACCEPTED MANUSCRIPT

ACCEPTED MANUSCRIPT

Abbreviations

cFe- colloidal iron (10 kDa < cFe < 0.2 µm)
CLE-ACSV- competitive ligand exchange adsorptive cathodic stripping voltammetry
CFF- cross flow filtration
dFe- dissolved iron (< 0.2 µm)
Fe- iron
ID-ICP-MS- isotope dilution inductively-coupled plasma mass spectrometry
sFe- soluble iron (< 10 kDa)

ACCEPTED MANUSCRIPT

ACCEPTED MANUSCRIPT

Abstract

The size partitioning of dissolved iron and organic iron-binding ligands into soluble and colloidal phases was investigated in the upper 150 m of two stations along the GA03 U.S. GEOTRACES North Atlantic transect. The size fractionation was completed using cross-flow filtration methods, followed by analysis by isotope dilution inductively-coupled plasma mass spectrometry (ID-ICP-MS) for iron and competitive ligand exchange-adsorptive cathodic stripping voltammetry (CLE-ACSV) for iron-binding ligands. On average, 80% of the 0.1-0.65 nM dissolved iron (<0.2 μm) was partitioned into the colloidal iron (cFe) size fraction (10 kDa < cFe < 0.2 μm), as expected for areas of the ocean underlying a dust plume. The 1.3-2.0 nM strong organic iron-binding ligands, however, overwhelmingly (75-77%) fell into the soluble size fraction (<10 kDa). As a result, modeling the dissolved iron size fractionation at equilibrium using the observed ligand partitioning did not accurately predict the iron partitioning into colloidal and soluble pools. This suggests that either a portion of colloidal ligands are missed by current electrochemical methods because they react with iron more slowly than the equilibration time of our CLE-ACSV method, or part of the observed colloidal iron is actually inorganic in composition and thus cannot be predicted by our model of unbound iron-binding ligands. This potentially contradicts the prevailing view that greater than 99% of dissolved iron in the ocean is organically complexed. Untangling the chemical form of iron in the upper ocean has important implications for surface ocean biogeochemistry and may affect iron uptake by phytoplankton.

ACCEPTED MANUSCRIPT

1. Introduction

Since iron (Fe) is known to limit primary production in large portions of the global ocean (Boyd et al., 2007; Martin et al., 1994; Moore et al., 2002), much of the exploration of marine Fe biogeochemistry is focused on the association between Fe fluxes in the surface ocean and biological uptake of dissolved Fe by microorganisms. The biological utilization of Fe during photosynthesis, nitrogen fixation, and respiration (Morel et al., 2003; Sunda, 2012) unequivocally links Fe biogeochemistry to the global carbon cycle and ultimately climate. However the conversion efficiency of "new" dissolved Fe from lithogenic source to cell-assimilated form (Morel et al., 2008; Shaked et al., 2005) is ultimately controlled by the many elusive physicochemical forms that dissolved Fe assumes. Processes such as scavenging/precipitation, Fe exchange, and photochemistry are both sensitive to and responsible for controlling the physicochemical speciation of Fe, and thus the chemical reactivity and fate of dissolved Fe is changed at each step along its transformation pathway.

Much has been learned about the physicochemical form of dissolved Fe over the last several decades. Dissolved Fe (dFe, here defined as <0.2 µm) has a broad size distribution composed of both "truly dissolved" soluble Fe (sFe <10 kDa) and "very small particulate" colloidal Fe (10 kDa < cFe < 0.2 µm) size fractions, with colloidal Fe contributing 0-90% of total dFe across the global ocean (Bergquist et al., 2007; Chever et al., 2010; Fitzsimmons and Boyle, 2014b; Fitzsimmons et al., in press; Nishioka et al., 2001; Ussher et al., 2010; Wu et al., 2001). Incubation studies have shown that while a limited number of cFe forms are highly bioavailable (such as exopolymeric saccharides, Hassler et al., 2011b), sFe is typically preferred and is taken into the cell much faster than cFe (Chen et al., 2003; Chen and Wang, 2001; Wang and Dei, 2003). Crystalline inorganic cFe (such as nanoparticulate Fe oxyhydroxide) is not directly available to marine phytoplankton at all (Rich and Morel, 1990; Wells et al., 1983),

ACCEPTED MANUSCRIPT

although freshly precipitated amorphous cFe nanoparticles have been found to be somewhat bioavailable to coastal species (Kuma and Matsunaga, 1995). In addition to this physical description of dFe speciation, studies using competitive ligand exchange electrochemical measurements have suggested that >99% of marine dFe, including both soluble and colloidal sized species, is complexed by organic ligands (Rue and Bruland, 1995; van den Berg, 1995; Wu and Luther, 1995). It is generally accepted that it is this binding of marine Fe by organic complexes that bolsters dFe concentrations above the ~0.1 nM inorganic solubility limits of organic-free seawater (Liu and Millero, 2002; Millero, 1998). While a few marine Fe-binding organic ligands have been identified as hydroxamate siderophores (Mawji et al., 2011; Velasquez et al., 2011; Vraspir and Butler, 2009), structurally characterized ligands only comprise a small percentage of the total dFe pool (<5%), and in general the identity of marine Fe-binding ligands is largely unknown (Gledhill and Buck, 2012).

However, the finding that nearly all marine dFe is organically bound is only an inference that relies on the assumption of thermodynamic equilibrium between dFe and dissolved Fe-binding ligands during electrochemical analysis and in the open ocean. Additionally, electrochemical characterization of Fe-binding ligands is somewhat limited, as only the Fe-binding ligands that are kinetically labile over the period of equilibrium with the added ligand can be detected, causing any refractory forms of dFe to be measured as a strong, Fe-bound ligand. In fact, Town & van Leeuwen (2005) asserted that kinetic limitation should prohibit many of the Fe-complexes detected by electrochemistry from being organic in composition, which precipitated an active debate on what is actually measured in competitive ligand exchange electrochemical measurements. Despite the shortcomings of electrochemical measurements, they are currently the predominant source of information on the chemical speciation of marine dFe,

ACCEPTED MANUSCRIPT

since almost no studies have conducted direct chemical speciation measurements, largely because of analytical hurdles. One analysis of colloidal Fe composition by energy dispersive spectroscopy showed that open ocean cFe is mostly organically bound (Wells and Goldberg, 1992), while in contrast a recent study using synchrotron technology demonstrated that a portion of the surface colloidal Fe underlying dust plumes in the Southern Ocean is inorganic, composed of tiny fragments of magnetite (von der Heyden et al., 2012). Thus, while the long-standing assumption is that the overwhelming majority of dFe is bound by strong organic Fe-binding ligands, there is a possibility that some dFe, especially in the colloidal phase, is inorganically bound (nanoparticulate). This might be especially true in regions where continental Fe sources are significant, such as underlying dust plumes, downstream of hydrothermal vents, near the continental margin, in regions with abundant glacial meltwater, *etc.*(Fitzsimmons et al., in press).

The chemical composition of dFe affects productivity the most in the upper ocean where phytoplankton are active, and simultaneously the surface ocean receives atmospheric dust deposition of Fe, arguably the most significant Fe input to the ocean (Jickells et al., 2005; Mahowald et al., 2005). The solubility of aerosol Fe is variable and depends on a suite of factors including aerosol composition, source (anthropogenic or crustal), and size, as well as seawater pH and Fe-binding ligand concentration (Baker and Croot, 2010). Studies of the size partitioning of dFe have consistently shown that in the surface ocean underlying dust plumes, dFe is predominantly colloidal in size (Bergquist et al., 2007; Fitzsimmons and Boyle, 2014b; Fitzsimmons et al., in press; Ussher et al., 2010; Wu et al., 2001), while in the surface ocean of low-dust regions, the smaller soluble size fraction dominates the dFe pool (Boye et al., 2010; Chever et al., 2010; Nishioka et al., 2003; Wells, 2003). Colloidal Fe has also been shown to be

ACCEPTED MANUSCRIPT

the dominant Fe size fraction yielded in seawater leaches of natural dust (Aguilar-Islas and Mehalek, 2013; Aguilar-Islas et al., 2010).

These patterns raise two important questions: what is the physicochemical speciation of the abundant cFe in the surface ocean after recent dust deposition, and how much of this dust-derived cFe is bioavailable? It is possible for the dust-derived surface cFe maximum to have any of three possible chemical compositions: Fe bound by colloidal-sized organic ligands after solubilization from dust, colloidal-sized fragments of dust that physically separated from aerosol particles upon impact with the surface ocean (resulting in an inorganic cFe composition of the same composition as the dust), or Fe that was initially solubilized from dust in the surface ocean but then re-precipitated *in situ* and aggregated to colloidal size (also resulting in an inorganic cFe composition, presumably amorphous Fe oxyhydroxides and mixed organic/inorganic precipitates). Each of these three Fe forms has a unique chemical lability and thus would have a different propensity for scavenging, aggregation, or biological uptake. Thus, the distinction between these physicochemical forms is at the crux of the problem linking dust deposition to biological uptake of dFe.

In this paper, we explore the physicochemical speciation of dFe in the upper 150 m of the high-dust North Atlantic Ocean where dFe falls predominantly into the colloidal size fraction, as is typical of dusty marine environments (Fitzsimmons et al., in press). Using an analysis of the Fe-binding ligand concentration and strength of both the soluble and dissolved Fe pools, we aim to consider whether there could be a natural inorganic component to the colloidal Fe pool of the surface ocean of this dusty environment, which could provide an exception to the prevailing view that >99.9% of dFe is believed to be bound by organic ligands.

ACCEPTED MANUSCRIPT

2. Methods

2.1 Sample collection

Seawater samples from the upper 150 m of the ocean were collected from two stations on the U.S. GEOTRACES GA03 North Atlantic Zonal Transect 2011 cruise (Nov-Dec 2011): Station 10 at 31.933°N, 64.733°W near the Bermuda Atlantic Time Series (BATS) site and Station 23 at 18.39°N, 26.765°W near the Cape Verde Islands (Figure 1). Hydrographic parameters defining these regions were measured using a Seabird *SBE9+* CTD and an *SBE43* dissolved oxygen sensor, which was calibrated by Winkler titrations (Langdon, 2010). Trace metal clean seawater was collected using the U.S. GEOTRACES GO-FLO rosette by the methods described in Cutter and Bruland (2012). Briefly, GO-FLO bottles were carried individually into an ISO 5-rated clean van, where the seawater was filtered through pre-cleaned 0.2 µm Pall Acropak-200™ Supor® capsule filters under ~0.4 atm of HEPA-filtered air. Surface samples were collected using the GeoFish system (Bruland et al., 2005), which employs all-perfluoroalkoxy alkane (PFA) tubing attached to a vane that coasted at ~3 m depth suspended from a boom off the starboard side of the ship during forward ship motion of up to 12 knots. An all-PFA diaphragm pump drew clean seawater through this system at ~0.5 atm pressure, and filtration was completed first through a 0.45 µm Osmonics (Teflon™, MSI) filter and then through a 0.2 µm polycarbonate track etched filter mesh held in a polypropylene housing (Nuclepore™). Filtrates were taken into acid cleaned 4L low density polyethylene (LDPE) bottles after three bottle rinses. Sub-samples of this 4L were taken into 30 mL high density polyethylene (HDPE) bottles for Fe concentration analysis and into 500 mL fluorinated polyethylene (FLPE) bottles for the dFe-binding ligand analysis. LDPE and HDPE bottles were cleaned in 1 M reagent grade HCl, including an overnight heating to 60°C, after which they were

ACCEPTED MANUSCRIPT

rinsed and filled with pH 2 ultrapure acid until use (Fitzsimmons and Boyle, 2012). FLPE bottles were cleaned in 3 M trace metal grade HCl for a month and then were conditioned with ultra clean Milli-Q water for more than a month prior to sample collection in order to remove all acid residue (Buck et al., 2012).

To collect the sFe fraction (< 10 kDa), the remainder of the 4L filtrates were immediately ultrafiltered through an all-Teflon cross-flow filtration (CFF) system in static mode (CFF filter cleaning and ultrafiltration protocol described in detail in Fitzsimmons and Boyle, 2014a). Briefly, a Millipore Pellicon XL (PLCGC) 10 kDa regenerated cellulose CFF membrane was employed, and 300-350 mL of sample seawater was first flushed through the acid-cleaned system to condition the membrane and CFF tubing against Fe sorption, after which the permeate stream was collected as the sFe or sFe-ligand sample. After 0.2 µm filtration and 10 kDa ultrafiltration, Fe-binding ligand samples were frozen un-acidified until analysis, and all Fe concentration samples were acidified to pH 2 using 6N reagent grade hydrochloric acid that had been purified from reagent grade acid by four distillations in a Vycor still (Fe concentration ~ 0.1 nmol/kg).

Additional seawater for determination of the mass balance of Fe-binding ligands through the CFF system was collected from the surface Pacific Ocean at 22.75°N, 158°W (Station ALOHA) on 19 July 2013 on the HOE-PhoR-II cruise supported by the Center for Microbial Oceanography: Research and Education (C-MORE). Seawater was pumped from 15 m depth through an all-PFA diaphragm pump through acid-cleaned tubing into a 0.2 µm Acropak-200 filter (Pall) and then into acid-cleaned 8 L LDPE bottles. Subsamples were collected for dFe (<0.2 µm) and ultrafiltered for sFe (<10 kDa) concentration and dFe-binding ligand analysis and preserved as described above for the GA03 cruise.

ACCEPTED MANUSCRIPT

2.2 Fe analyses

3-10 months after acidification, dFe and sFe samples were analyzed in triplicate for their Fe concentration at MIT by isotope dilution inductively-coupled plasma mass spectrometry (ID-ICP-MS) on a hexapole collision cell IsoProbe multi-collector ICP-MS (Lee et al., 2011). The ID-ICP-MS method employs a ^{54}Fe-spike and batch pre-concentration with nitrilotriacetate resin (NTA, Qiagen). cFe was calculated as the difference between dFe and sFe. Fe procedural blanks were measured by many repeat analyses of 300 µL aliquots of a large volume seawater sample taken from the surface ocean at the SAFe station that has a known, low-Fe concentration (0.05 nmol/kg). The procedural blanks averaged 0.044 nmol/kg with a typical standard deviation over a single day's analysis of 0.009 nmol/kg; thus, the reported detection limit is 0.027 nmol/kg. Comprehensive lab analyses of the SAFe S seawater for dFe during the period of these analyses averaged 0.101±0.009 nmol/kg (Bottles 17 and 318, n=6), which agrees well with the consensus value of 0.093±0.008 nmol/kg. Similarly, SAFe D2 standard for dFe during the period of these analyses averaged 0.911±0.018 nmol/kg (Bottle 446, ±1SD, n=15), which also agree well with the consensus value of 0.933±0.032 nmol/kg. Consensus values cited here were updated in May 2013 (www.geotraces.org/science/intercalibration).

2.3 Fe-binding ligand analyses

Measurements of dFe and sFe-binding ligand concentrations and binding strengths were made by competitive ligand exchange-adsorptive cathodic stripping voltammetry (CLE-ACSV) on a BioAnalytical Systems (BAS*i*) Controlled Growth Mercury Electrode coupled to a BAS*i* Epsilon ε2 voltammetric analyzer by the methods described in Buck et al. (2007). Briefly,

ACCEPTED MANUSCRIPT

samples stored frozen for 4-12 months since collection were gently thawed at 4°C and then shaken vigorously before analysis. Next, 10 mL sample aliquots were buffered to pH 8.2 (NBS scale) with a borate-ammonium buffer in PFA vials (Savillex) that had been previously conditioned to the anticipated Fe addition. Titration Fe additions were made at concentrations ranging from 0-7.5 nM and were allowed to equilibrate for 2 hours before the addition of the added ligand, salicylaldoxime (SA), at concentrations of 25 or 32.3 µM ($\alpha_{Fe(SA)_2}$ = 60 or 100). After a 15 minute equilibration with SA, the $Fe(SA)_2$ complex was adsorbed to the mercury drop at 0 V for 2-5 minutes and then stripped at 0.03 V/s using differential pulse mode to a final potential of -0.85 V. Raw titration data were interpreted for their Fe-binding ligand concentration ([L]) and ligand conditional stability constants ($K^{cond}_{FeL,Fe'}$) using the van den Berg/Ružić (Ružić, 1982; van den Berg, 1982) and the Scatchard (Mantoura and Riley, 1975; Scatchard, 1949) linearization techniques, the results of which were averaged to obtain the reported values and error estimates. Sensitivities were determined by internal calibration at the end of the titration, when all ligands are titrated. An $\alpha_{Fe'}$ of 10^{10} was assumed in the Fe speciation calculations. Note here that all K values listed in this paper are conditional stability constants even when the "K^{cond}" designation has been dropped for convenience.

2.4 Fe-ligand mass balance determination

The mass balance of Fe-binding ligands following CFF was determined on the 15 m Station ALOHA seawater in order to assess the potential loss of ligands during this ultrafiltration, since ~25-30% loss of dFe has been observed using the same system (Fitzsimmons and Boyle, 2014a). Station ALOHA samples for Fe concentration and Fe-binding ligand concentration and strength were collected and analyzed from the dissolved (< 0.2 µm),

ACCEPTED MANUSCRIPT

CFF permeate (assumed to be sFe), and CFF retentate (containing some sFe and some cFe) streams. With the permeate and retentate flow rates calibrated identically at 12.5 mL/min each, the concentration factor (CF) in static mode was calculated to be 2.0 using the following equation:

$$CF = \frac{\text{initial sample volume}}{\text{final retentate volume}} = \frac{\text{permeate volume + retentate volume}}{\text{retentate volume}} \quad (1)$$

Under ideal permeation conditions where the membrane does not preferentially retain any soluble compounds (permeation coefficient = 1, Schlosser and Croot, 2008), the permeate solution should define the sFe and the sFe-binding ligand concentrations (<10 kDa). However, in solutions containing cFe, the Fe and Fe ligand concentrations in the retentate solution must be corrected for the presence of sFe and the degree of CFF concentration in order to calculate the true cFe and cFe-ligand concentrations, as follows:

$$cFe = \frac{[Fe]_{retentate} - [Fe]_{permeate}}{CF} \quad (2)$$

To determine mass balance, the sFe (permeate) and cFe (Equation 2) concentrations were compared to the dFe (< 0.2 µm solution originally fed into the CFF system) concentration, and the same was completed for the Fe-binding ligand concentrations.

3. Results

Large volume seawater samples containing the dissolved (<0.2 µm) and soluble (<10 kDa) Fe size fractions were collected in two regions of the North Atlantic Ocean (Figure 1): the region near the Cape Verde Islands (Station 23) and the subtropical gyre region near Bermuda (Station 10). These locations were chosen for two reasons. First, we aimed to sample variable dust loading and composition in the surface ocean: Station 10 near Bermuda experienced ~2 ng/m^3 aerosol Fe loadings with a "marine/North American" aerosol source and an Fe solubility

ACCEPTED MANUSCRIPT

of 3.5% (in instantaneous water leachate), while Station 23 near Cape Verde experienced much higher aerosol Fe loadings of ~3600 ng/m^3 coming from a "North African" source with a lower Fe solubility of ~0.4% (HYSPLIT back trajectories are shown in Figure S1 and were determined using Draxler and Rolph, 2014; aerosol Fe loadings reported from Shelley et al., in review; aerosol Fe solubility reported from Rachel Shelley and William Landing, personal communication). When aerosol Fe loading and solubility are both considered, the aerosol inputs of dFe to Station 10 should have been ~200 times lower than to Station 23. However, we note that even Station 10 receives significantly higher dust Fe loadings (0.5-30 nmol/m^3 Fe, Sedwick et al., 2007; Sholkovitz et al., 2009) than the traditional “low-dust” regions of the global ocean (e.g. the South Pacific at <0.01 ng/m^3 Fe, Wagener et al., 2008), and thus dust likely plays a major role in controlling Fe cycling in near-surface waters of both stations.

Second, we wanted to sample upper ocean regions with variable biological populations, biogeochemistry, and water mass structure (profiles in Figure 2, temperature-salinity diagrams in Figure S2). Station 10 receives influences from the Gulf Stream southern recirculation in the mixed layer (Talley et al., 2011), which extended to 88 m depth (Figure 2a), and then from Eighteen Degree Water (θ=18°C, salinity=36.5, O_2=200 µmol/kg; Worthington, 1959) extending from the bottom of the mixed layer to below 200 m depth. In contrast, station 23 is located where the Canary Current transitions into the North Equatorial current (Talley et al., 2011), bringing waters from the northeast to the southwest. This surface current extended through the mixed layer at 63m (Figure 2b), below which an influence of the salty Subtropical Underwater (STUW: θ=25°C, salinity>37) dominated through 95 m depth. Below ~100 m depth North Atlantic Central Water (NACW) dominates all the way through ~600 m depth. From Figure 2 it is clear that station 10 was situated more in the subtropical gyre with a depressed pycnocline to >350 m

ACCEPTED MANUSCRIPT

depth, while station 23 was situated south of the gyre, with a much shallower pycnocline starting at ~100 m depth, and received influences of oxygen minimum zone (OMZ) waters below ~250 m depth.

This paper will focus on results from size-fractionated soluble and dissolved Fe and Fe-binding ligand samples collected in the North Atlantic. For perspective on the Fe biogeochemistry occurring in the North Atlantic during the time of the GA03 cruise, please see Hatta et al. (in press) for general dFe biogeochemistry, Conway and John (Conway and John, 2014) for quantification of Fe sources, Fitzsimmons et al. (in press) for a discussion of the dFe size partitioning into soluble and colloidal phases, Shelley et al. (in review) for marine aerosol Fe fluxes, and Buck et al. (in review) for the distribution of dissolved organic Fe-binding ligand concentrations and strengths.

3.1 Size partitioning of dissolved Fe and Fe-binding ligands

We evaluated the size-partitioning of dissolved Fe and Fe-binding ligands in the upper 150 m of the North Atlantic Ocean in order to explore the physicochemical speciation of dust-derived dFe phases. As shown in Figure 3, dFe concentrations were elevated (<0.4 nM) in the surface ocean of both stations, and dFe was ~80% partitioned into the colloidal size fraction (10 kDa < cFe < 0.2 µm). This surface dominance of dFe by colloidal-sized species was consistent across the entire GA03 North Atlantic transect (Fitzsimmons et al., in press), regardless of relative dust Fe loading so long as dust was abundant (minimum Fe concentrations in aerosols of 1 ng/m^3; Shelley et al. in review). This was used as evidence that aerosol-derived Fe is preferentially maintained in the colloidal size fraction, consistent with other studies demonstrating that cFe dominates in dusty surface ocean regions (Bergquist et al., 2007;

ACCEPTED MANUSCRIPT

Fitzsimmons and Boyle, 2014b; Wu et al., 2001). Below the surface at the 70-90 m deep chlorophyll maximum (DCM) cFe decreased to a minimum concentration, another feature typical of North Atlantic dFe size partitioning (Fitzsimmons et al., in press).

Organic Fe-binding ligands, however, were overwhelmingly partitioned into the soluble size fraction (Figure 3, Tables 1 and 2). Two ligand pools were detected at each of the depths measured (L_1 is the stronger ligand class, L_2 is weaker, and $L_T = L_1 + L_2$), and Fe ligand concentrations in the soluble and dissolved size fractions always exceeded their respective Fe concentrations so that the dissolved and soluble Fe ligand concentrations reported are free ligands not bound to Fe (excess L_1 concentrations were 1.2-2.0 nM soluble and 1.2-2.5 nM dissolved at Station 10; 1.0-1.6 nM soluble and 1.2-1.6 nM dissolved at Station 23). While excess L_1 ligand concentrations are typical of open ocean conditions (Buck et al., 2012; Gledhill and Buck, 2012) and thus not surprising in the dissolved and soluble phases of this study, colloidal L_1 (calculated as dissolved L_1 – soluble L_1) had lower concentrations than cFe at many depths, resulting in negative excess colloidal L_1 concentrations (Figure 3). This reinforces the major result that colloidal ligands were very low in concentration and also suggests that the cFe present was bound to weaker ligands than the sFe.

Electrochemical ligand detection is a function of the analytical window utilized, which is established by the concentration and binding strength of the competing ligand added during the titration, defined in this study as $\alpha_{Fe(SA)2} = \beta^{cond}_{Fe(SA)2,Fe'} * [SA]^2$. At the lower analytical window used in this study ($\alpha_{Fe(SA)2} = 60$, Table 1), both ligand classes were preferentially partitioned into the soluble size fraction: soluble L_1 ligands ranged from 1.0-2.1 nM and averaged 77±17% of the dissolved L_1 ligands (1.65-2.65 nM) at station 10 and 75±13% of the dissolved L_1 (1.35-1.95 nM) at station 23, while total (L_1+L_2) soluble ligands ranged from 2.5-8.3 nM and averaged

ACCEPTED MANUSCRIPT

78±7% of the total dissolved ligands at station 10 (3.0-9.0 nM) and 86±5% of the total dissolved ligands at station 23 (6.8-8.9 nM). At the higher analytical window ($\alpha_{Fe(SA)2}$ = 100, Table 2) where stronger ligands could be detected, the pattern of excess soluble ligands was the same: soluble L_1 ligands comprised 77±12% and 93±7% of the total L_1 ligands detected at stations 10 and 23, respectively. Only at the DCM of station 10 did colloidal ligands comprise the greatest portion of total dissolved ligands (Figure 3).

The $K^{cond}_{FeL,Fe}$, values for the two ligand classes had variable size partitioning patterns, both within a single station and across the two stations (Figure 3). At station 10, log $K^{cond}_{FeL,Fe}$, values were not significantly different between the two size fractions, except near the DCM where log K_1 was greater at ~13 for the soluble size fraction and nearer to ~12 for the total dissolved size fraction, indicating that colloidal ligands were weaker at this depth. At station 23, log K_2 values were identical between the two size fractions, while log K_1 values were slightly higher in the colloidal fraction than in the soluble fraction at most depths.

Using the size partitioned Fe-ligand binding strength and concentration data together, we determined the capacity for the free Fe-binding ligands in each size fraction to bind Fe, $\alpha_{FeL'}$:

$$\alpha_{FeL'} = 1 + ([eL_1] * K_1) + ([L_2] * K_2) \quad (3)$$

where the concentration of excess L_1 ($[eL_1]$) is the L_1 not already bound to Fe:

$$[eL_1] = [L_1] - [Fe] \quad (4)$$

This $\alpha_{FeL'}$ was calculated for each size fraction and is shown in Figure 3. The total dissolved $\alpha_{FeL'}$ was greater than the soluble $\alpha_{FeL'}$ at most depths of station 23, indicating that the colloidal ligands had at least some capacity to bind Fe. Only at the deepest (129 m) depth of station 23 was the dissolved $\alpha_{FeL'}$ the same as the soluble $\alpha_{FeL'}$, indicating that the colloidal ligands had no capacity to bind new Fe at this depth. At the DCM of station 10, in contrast, the soluble $\alpha_{FeL'}$

ACCEPTED MANUSCRIPT

was greater than the dissolved $\alpha_{FeL'}$, which was related to the greater log$K^{cond}_{FeL,Fe}$, values calculated for the soluble ligands than the total dissolved ligands at these depths (Table 3).

The primary objective of this study, however, was to determine whether the size partitioning of organic Fe-binding ligands in the upper ocean would predict the observed size partitioning of dFe. Thus, following Cullen *et al*. (2006), we modeled the fraction of total dFe expected to exist in the soluble phase at equilibrium with the observed size fractionated ligands:

$$\frac{\mathrm{Fe_{sol}}}{\mathrm{Fe_{diss}}} = \frac{(\alpha_{\mathrm{FeL'}})_{\mathrm{sol}}}{(\alpha_{\mathrm{FeL'}})_{\mathrm{diss}}} = \frac{[(K_1*[eL_1])+(K_2*[L_2])]_{\mathrm{sol}}}{[(K_1*[eL_1])+(K_2*[L_2])]_{\mathrm{diss}}} \quad (5)$$

If dFe is organically bound to ligands with the same concentration and strength as calculated using the $\alpha_{FeL'}$value of the observed free ligands, then the modeled partitioning should match the observed dFe partitioning (in this case, the left-most and the right-most panels of Figure 3 should match).

We also compared the modeled and observed soluble Fe partitioning fractions in Figure 4, and the observed sFe fractions all fell below the modeled-observed 1:1 line, indicating that the size partitioning of organic ligands as measured by electrochemistry does not predict the observed dFe size partitioning in the upper ocean of either station.

3.2 Mass-balance of Fe-binding ligands using CFF

It is well known that Fe recovery during CFF can be low (Reitmeyer et al., 1996), and using the same low-surface area, regenerated cellulose cross flow filtration system as in this study, Fitzsimmons and Boyle (2014a) suffered a 25-30% dFe loss to the surface and/or pores of the CFF filter. They used various lines of evidence to propose that it was only the colloidal fraction that was lost/trapped in the filter membrane, while sFe was fully recovered in the

ACCEPTED MANUSCRIPT

permeate solution. It was important to prove that this was also true for the free and bound Fe-binding ligand fractions in order to provide accurate calculations in this study.

Thus, the mass balance of Fe-binding ligands during CFF was determined at 15 m depth at Station ALOHA (22.75°N, 158°W) in the Pacific Ocean (Table 4). Fe concentration and Fe-binding ligand concentration and strength were measured for the permeate, retentate, and initial CFF feed solutions. The soluble Fe and Fe-binding ligand concentrations were assumed to be equal to that found in the permeate (ideal permeation characteristics of the CFF membrane were assumed here, as they were determined for Fe concentrations in Fitzsimmons and Boyle, 2014a), and the initial CFF feed solution was set equal to the "dissolved" <0.2 µm fraction. Colloidal Fe and ligand concentrations derived from the CFF system were calculated using Equations 1-2. Using the definitions of soluble and colloidal sizes, soluble Fe (defined here as <10 kDa) plus colloidal Fe (defined here as between 10 kDa and 0.2 µm) should equal dissolved Fe (defined as < 0.2 µm). Thus, the measured "soluble+colloidal" concentration was compared to the measured dissolved concentration in the CFF feed solution to determine the mass balance:

$$\%\ \text{Recovery} = \frac{[\text{Soluble}]_{\text{meas}} + [\text{Colloidal}]_{\text{meas}}}{[\text{Feed solution}]_{\text{meas}}} * 100\% \quad (6)$$

These calculations were completed for the Fe concentration, ligand concentration, and excess ligand concentration (Table 4). The Fe recovery from the CFF system was low at 54±27%, which is within error of the average 70-75% mass balance for Fe concentration recorded using the same system by Fitzsimmons and Boyle (2014a) across several sampling sites in the Pacific and Atlantic Oceans. The large 27% error is attributed to the extremely low concentrations of sFe (0.039±0.008) measured at this station. The total ligand recovery was quite similar at 65±27%, and when only the excess ligand is considered, the recovery was 69±34%. Since the recoveries were so similar between Fe and L concentrations, we can safely assume that

ACCEPTED MANUSCRIPT

the same mechanism that causes cFe loss to the CFF membrane, which Fitzsimmons and Boyle (2014a) attributed to either cFe accumulation on the CFF membrane or cFe entrapment in the pores of the CFF membrane, also causes free colloidal ligand losses to the CFF membrane. Free soluble ligands, in contrast, likely permeate the membrane completely. While we cannot prove this conclusively as Fitzsimmons and Boyle (2014a) did for deep Atlantic sFe, the fact that the soluble ligand fraction accounted for the majority of the dissolved ligand pool supports the conclusion that the majority of soluble ligands are recovered by CFF. This indicates that the size partitioning conclusions drawn in this study using the dissolved and soluble (permeate) ligand measurements are valid; only retentate ligand measurements are affected by poor recovery and should be avoided. Colloidal ligand concentrations can thus be calculated using the following equation (instead of Equation 2):

$$[\text{colloidal L}] = [\text{dissolved L}] - [\text{soluble L}] \quad (7)$$

4. Discussion

The results of this study demonstrate that while dFe falls predominantly into the colloidal size fraction in surface waters underlying the North African dust plume, the excess ligands in these same waters are instead partitioned into the soluble size fraction. This pattern was repeated at the two stations studied in the North Atlantic Ocean, which both received significant dust fluxes that varied two orders of magnitude in Fe loading and also in aerosol source. Variable size fractionation of Fe-binding ligands with depth and location has also been observed in the upper 200m by Boye *et al.* (2010) in the Southern Ocean (200 kDa filter used), by Thuroczy *et al*. (2010) in the Northeast Atlantic Ocean (1000 kDa filter used), and by Cullen *et al*. (2006) in the North and South Atlantic Oceans (0.02 µm filter used).

ACCEPTED MANUSCRIPT

With these results, we aimed to explore the chemical composition of the colloidal Fe maximum found in surface ocean regions underlying dust plumes, particularly whether it is organically or inorganically bound. We based our interpretation of these size fractionated ligand results on the hypothesis that if the size partitioning of free surface Fe-binding ligands into soluble and colloidal fractions predicted the observed surface dFe size partitioning, then surface dFe is likely bound by organic ligands. It is clear from the results of Figures 3 and 4 that this was not the case: observed free Fe-binding ligands were primarily soluble, while observed dFe was mostly colloidal in size. This does not preclude an organic composition of the colloidal Fe in the dusty surface North Atlantic. However, it must mean that either (1) we are missing a fraction of free colloidal ligands in our electrochemical measurements, or (2) some portion of the cFe in the surface ocean is inorganic in composition (not controlled by equilibrium with a size-partitioned set of free organic ligands, as our calculations assume).

To evaluate these possibilities, we must consider the assumptions involved in the electrochemical measurements of Fe binding ligands and the $\alpha_{FeL'}$ calculations (Equation 5, Figure 4) used in this study. First, unbound ligands can only be detected using CLE-ACSV if they are able to exchange with Fe on the timescale of the analytical equilibrium (in this case, 2 hours with added Fe and 15 minutes with SA). Thus, any kinetically-inhibited free ligands would not be detected by this CLE-ACSV method, and our measured ligand concentrations could be underestimated. Other CLE-ACSV methods use longer equilibration times (8-12 hours) with both the metal additions (e.g., Croot and Johansson, 2000) and the added ligand (e.g., Gledhill and van den Berg, 1994). The longer equilibration times may allow for the detection of additional ligands (likely weaker ligands) with sluggish kinetics so long as the added ligand concentrations are not too high to out-compete the weaker ligands in the sample.

ACCEPTED MANUSCRIPT

We aimed to estimate what concentration of "kinetically-inhibited" colloidal-sized free ligands would be required to predict the observed dFe size partitioning. The majority of known colloidal Fe-binding ligands in the marine environment fall into the weaker (L_2) ligand class, such as polysaccharides (Hassler et al., 2011a) and humic-like substances (Laglera and van den Berg, 2009). Thus, we calculated the colloidal $K'^{cond}_{FeL,Fe}$ values (K_{coll}) for both L_1 and L_2 using the following equation:

$$[L]_{diss}K_{diss} = [L]_{sol}K_{sol} + [L]_{coll}K_{coll} \quad (8)$$

The colloidal ligand concentrations (calculated using Equation 7) and binding strengths (Equation 8) are tabulated in Table 5. In a few cases we were not able to calculate K_{coll} within the errors of our measurements.

Using these estimates, we calculated the concentration of "kinetically inhibited" colloidal-sized ligands at the calculated colloidal K_2 strength (Equation 8) that would be required to predict the observed dFe size partitioning (Table 5). The "missing colloidal ligand" concentrations at station 23 ranged from 0.03-7.63 nM, while the concentrations at station 10 were incalculable or reached very high concentrations that are not oceanographically consistent (13-60 nM). Notably, the lowest concentrations of "missing colloidal ligands" were calculated to occur at or immediately below the DCM, which is consistent with expectations, since it is at these depths that more of the dFe was of soluble size.

These missing ligands would need to be unbound colloidal-sized ligands that bind dFe in the ocean with kinetics more sluggish than the 2 hour equilibration time of our CLE-ACSV measurement. Our assumption that these ligands have a binding strength of the measured colloidal K_2 is the weakest assumption in our calculation. If the colloidal ligands were significantly stronger than assumed, our estimated missing colloidal [L] concentrations would be

ACCEPTED MANUSCRIPT

overestimated, which may explain the oceanographically inconsistent values calculated for station 10. Another possibility, however, is that a high concentration of relatively weak, inert colloidal ligands is reflected in the electrochemical data as a low concentration of a strong ligand instead. This might be the case if the cFe is partitioned into a ligand pool with no effective “free” ligand; in other words, the ligands binding the cFe do not have the capacity to take up any additional added Fe. It might only be possible to exchange Fe with this relatively “inert” pool if extremely long equilibration times are used or if higher analytical windows are employed, which would “outcompete” all other natural ligands in the sample (Kogut and Voelker, 2001). It was not clear from our use of slightly higher analytical window whether this was the case (Figure 4).

An alternative explanation is that a portion of the cFe is not in fact chelated by organic ligands but is inorganic, nanoparticulate cFe. Dust-derived surface dFe tends to be colloidal (Bergquist et al., 2007; Fitzsimmons and Boyle, 2014b; Fitzsimmons et al., in press), and while it could be bound by organic ligands of colloidal size, it could also be composed of physically eroded nanoparticulate fragments of dust and/or nanoparticulate Fe oxyhydroxides precipitated or aggregated *in situ* after aerosol Fe dissolves. This inorganic cFe would not be expected to adsorb to the electrochemical mercury drop nor exchange Fe with the added ligand, and thus electrochemistry would interpret this cFe as organically bound by a strong ligand (L_1). In this paper we modeled the predicted size partitioning of dFe using the size partitioning of the "excess" Fe-binding ligands; however, nanoparticulate Fe would not have an "excess" or "free" ligand pool that could represent it in these calculations. In other words, our Equation 5 calculations would not capture the "potential" to form nanoparticulate cFe that an unbound colloidal-sized ligand would. Thus, we would expect that if a significant portion of cFe was

ACCEPTED MANUSCRIPT

nanoparticulate, then we would see the exact results observed in Figure 3: ligand partitioning enriched in soluble-sized free compounds, while instead more of the dFe is colloidal.

However, we must consider the observation that the relative aerosol dFe input to the eastern basin at Station 23 was higher than at Station 10 in the western Atlantic, assuming the measured aerosol Fe loading and solubility (Shelley et al. in review). As a result of this, if cFe included a significant nanoparticulate component we might have expected more cFe and an additional "missing colloidal ligand" at Station 23 in the east than at Station 10 in the west. However, the observed size partitioning of dissolved Fe and Fe-binding ligands at both stations was the same, with no enhanced dust-derived effects at the dustier Station 23. One explanation for this inconsistency is that the aerosol Fe samples collected on this cruise were measured on 1-3 day timescales that are much shorter than the surface ocean residence time of dFe in the tropical North Atlantic (0.2 - 5 months; Bergquist and Boyle, 2006; Croot et al., 2004); thus, any dust deposition in the previous 5 months at Station 10 would still be evident in the dFe and Fe-binding ligands of surface waters but not in the real-time dust collection from the cruise. It is worth noting that the surface dFe concentration at both stations was elevated and similar in concentration (0.45-0.55 nM), likely reflecting recent aerosol Fe addition, and thus it might not be unreasonable to expect similar dust-driven patterns in dFe and Fe-ligand size partitioning at both stations. In fact, higher surface dissolved aluminum concentrations near Station 10 compared to Station 23 further support that aerosols significantly influence surface seawater chemistry at both stations (Measures et al., in press). Additionally, the higher dust loadings near the African continent serve not only to add dFe from dust but also to scavenge dFe onto the increased lithogenic particle loads falling through this water column, potentially creating a lower-than expected dFe addition when both dust source and scavenging are considered. These

ACCEPTED MANUSCRIPT

differences in sampling timescale, residence time, and influence of circulation/scavenging all may explain why dFe physicochemical speciation might not be very different between the two stations studied, despite the large apparent short-term differences in dust loading between Stations 10 and 23 measured during the cruise.

Alternatively, a lack of difference in dFe and Fe-binding ligand size partitioning between the two stations may suggest that it is actually the fact that the electrochemical methods that are missing a portion of the colloidal ligand pool that is to blame for the divergent size fractionation of Fe and Fe-binding ligands in the surface ocean, not an inorganic cFe phase. In fact, Cullen *et al*. (2006) observed the same Fe and Fe-ligand partitioning patterns (but to a lesser extent) in surface waters of the tropical Atlantic, and they concluded that electrochemical methods were missing an "inert" pool of colloidal Fe ligands. Our observed data deviates much more substantially from the ligand-modeled data than Cullen *et al*. (2006) observed, but this may be explained by the higher analytical window employed by Cullen *et al*. (2006), which would be better at capturing stronger ligands. A much higher competition strength was used in that study ($\alpha_{Fe(TAC)_x}$= 271) compared to those used here ($\alpha_{Fe(SA)_2}$= 60, 100), and in fact the higher analytical window in this study compares slightly better with the measured Fe partitioning (Table 3). This is an indication that at least some portion of the colloidal ligand pool may be very strong - either a very strong organic Fe-binding ligand of colloidal size or a relatively inert inorganic cFe species.

In addition to a kinetic mechanism of poor chemical lability, a steric hindrance may also prevent the cFe ligands from being detected. In (1994), Mackey and Zirino presented the "onion model" in which trace metals in the ocean are bound by concentric layers of organic compounds held together by hydrogen and other coordination bonds. Thus, Fe may become sterically

ACCEPTED MANUSCRIPT

"trapped" inside a colloidal-sized organic matrix (which it does not have to bind particularly strongly to) that passes through our 0.2 µm filters and so is detected as dFe but is physically prevented from exchanging with the added ligand. While they might bind Fe in nature given time and the physical mixing of the surface ocean, these same "onion" organic compounds in their unbound form in our samples might not bind Fe strongly or quickly enough during the time of electrochemical equilibration to reveal their true "binding potential" in nature.

Thus, our size partitioning Fe ligand results showed that in surface locations underlying the North African dust plume, the labile organic Fe-binding ligands detected by CLE-ACSV were overwhelmingly partitioned into the soluble size fraction and do not predict the colloidal Fe composition of dFe observed. This suggests that the "binding potential" of a significant unbound colloidal ligand fraction is missed by current electrochemical techniques. We hypothesize that this "missing cFe" is composed of either nanoparticulate cFe (eroded dust fragments or *in situ* precipitated Fe oxyhydroxide aggregates) that has no "excess ligand"-like binding potential and is thus missed by our equilibrium physicochemical speciation model or a kinetically-slow or sterically-hindered organic ligand of colloidal size. In short, attempting to unveil the physicochemical speciation of an Fe atom upon new Fe input (such as a dust event) is challenging using electrochemical techniques because the true "binding potential" of colloidal ligands is not fully captured by the CLE-ACSV method used in this study. Further assessment and prediction of the composition and fate of dust-derived upper ocean dFe awaits new analytical methods that can chemically evaluate the binding environment of marine dFe species across their size spectrum.

5. Conclusions

ACCEPTED MANUSCRIPT

We evaluated the organic speciation of soluble (<10 kDa) and dissolved (<0.2 µm) Fe at a western and eastern station in the subtropical North Atlantic Ocean. We found that while the majority of the dFe was colloidal sized (10 kDa - 0.2 µm), most of the excess organic ligands were soluble sized, indicating that the size partitioning of labile organic Fe-binding ligands does not directly predict the observed size partitioning of dFe. While our ultrafiltration methods did lose 35±27% of the organic ligands to the cross flow filtration membrane, the soluble ligands were inferred to permeate the membrane fully, and thus the filtration method was not the cause of the ligand and Fe size divergence. Two possible explanations were offered. First, our CLE-ACSV method could be missing some of the free colloidal sized ligands if they are kinetically limited to reaction times greater than the equilibration time of our method (2 hours). This could be caused by true kinetic limitation or steric hindrance, and these ligands would have to be 1) unbound in the sample (or CLE-ACSV would detect them), 2) have the potential to bind Fe in nature (presumably composing a portion of the existing cFe), but 3) bind Fe slower than the timescale of CLE-ACSV equilibration (which is why they were not detected). Alternatively, some of the cFe could be inorganically composed, which would not offer an "excess" ligand pool that could model and predict the dFe size partitioning accurately, as attempted here.

Acknowledgements

We would like to thank Gonzalo Carrasco and Pete Morton for help collecting and filtering seawater on the GA03 North Atlantic GEOTRACES cruise, and we thank Rene Boiteau and Dan Repeta for use of their deck pump and Chris Hayes for help at sea on the HOE-PhoR-II cruise to Station ALOHA. We also thank the ODF team, who did such great work calibrating and tabulating the CTD data from the GEOTRACES cruise. We are indebted to C-MORE, the Chief

ACCEPTED MANUSCRIPT

Scientists of both cruises (Ed Boyle, Bill Jenkins, Greg Cutter, and Tara Clemente), and the officers and crew of the R/V *Kilo Moana* and the R/V *Knorr* for the opportunities to collect these samples at sea. Finally, we owe a large thanks to our two anonymous reviewers whose comments greatly improved the quality of this manuscript. J.N. Fitzsimmons was funded by a National Science Foundation Graduate Research Fellowship (NSF Award #0645960). Research funding was provided by the National Science Foundation (OCE #0926204 and OCE #0926197) and the Center for Microbial Oceanography: Research and Education (NSF-OIA Award #EF-0424599) to E.A. Boyle. R.M. Bundy was partially funded by NSF OCE-0550302 and NSF OCE-1233733 to K.A. Barbeau and an NSF-GK12 graduate fellowship.

ACCEPTED MANUSCRIPT

ACCEPTED MANUSCRIPT

Table Captions

Table 1. Iron and ligand partitioning at stations 10 and 23 at the lower analytical window ($\alpha_{Fe(SA)_2}$ = 60).

Table 2. Iron and ligand partitioning at stations 10 and 23 at the higher analytical window ($\alpha_{Fe(SA)_2}$ = 100).

Table 3. Modeled and measured iron and ligand partitioning according to Equation 3 for stations 10 and 23.

Table 4. Fe and Fe-binding ligand mass balance using cross flow filtration at 15 m depth at Station ALOHA in the Pacific Ocean.

Table 5. Mass balance-calculated colloidal ligand characteristics (at $\alpha_{Fe(SA)_2}$ = 60) and the additional "kinetically-inhibited" colloidal L_2 concentrations required to explain the observed dFe size partitioning at equilibrium.

ACCEPTED MANUSCRIPT

ACCEPTED MANUSCRIPT

Figure Captions

Figure 1. Sampling locations along the US-GEOTRACES 2011 transect for iron and iron-binding ligand partitioning studies.

Figure 2. Hydrography of the two North Atlantic study sites. The CTD traces from relevant sample depths are indicated in (a) for station 10 near Bermuda and (b) for station 23 near Cape Verde.

Figure 3: The partitioning of dFe and dissolved Fe-binding ligands in the dissolved (<0.2 µm, solid circles, solid line) and soluble (<10 kDa, open circles, dotted lines) at (a) station 10 (BATS) and (b) station 23 (near Cape Verde). The gray line is the fluorescence trace, and the maximum fluorescence is designated as the deep chlorophyll maximum (DCM). All error bars are ±1 standard deviation.

Figure 4. Measured sFe/dFe vs. modeled sFe/dFe at station 10 (near Bermuda, filled circles) and station 23 (near Cape Verde, crosses) at $\alpha_{Fe(SA)_2}$ = 60 and 100 (A and B, respectively). Modeled sFe/dFe was derived by dividing $\alpha_{soluble}/\alpha_{dissolved}$.

ACCEPTED MANUSCRIPT

ACCEPTED MANUSCRIPT

References

Aguilar-Islas, A.M. and Mehalek, A., 2013. Aerosol Fe solubility from field and lab-based leaching protocols, U.S. GEOTRACES post-cruise data workshop, Old Dominion University, Norfolk, VA.

Aguilar-Islas, A.M., Wu, J., Rember, R., Johansen, A.M. and Shank, L.M., 2010. Dissolution of aerosol-derived iron in seawater: Leach solution chemistry, aerosol type, and colloidal iron fraction. Marine Chemistry, 120(1-4): 25-33.

Baker, A.R. and Croot, P.L., 2010. Atmospheric and marine controls on aerosol iron solubility in seawater. Marine Chemistry, 120: 4-13.

Bergquist, B.A. and Boyle, E.A., 2006. Dissolved iron in the tropical and subtropical Atlantic Ocean. Global Biogeochemical Cycles, 20(1): 14.

Bergquist, B.A., Wu, J. and Boyle, E.A., 2007. Variability in oceanic dissolved iron is dominated by the colloidal fraction. Geochimica Et Cosmochimica Acta, 71(12): 2960-2974.

Boyd, P.W. et al., 2007. Mesoscale iron enrichment experiments 1993-2005: Synthesis and future directions. Science, 315(5812): 612-617.

Boye, M. et al., 2010. Significant portion of dissolved organic Fe complexes in fact is Fe colloids. Marine Chemistry, 122(1-4): 20-27.

Bruland, K.W., Rue, E.L., Smith, G.J. and DiTullio, G.R., 2005. Iron, macronutrients and diatom blooms in the Peru upwelling regime: brown and blue waters of Peru. Marine Chemistry, 93: 81-103.

Buck, K.N., Lohan, M.C., Berger, C.J.M. and Bruland, K.W., 2007. Dissolved iron speciation in two distinct river plumes and an estuary: Implications for riverine iron supply. Limnology & Oceanography, 52(2): 843-855.

Buck, K.N. et al., 2012. The organic complexation of iron and copper: an intercomparison of competitive ligand exchange-adsorptive cathodic stripping voltammetry (CLE-ACSV) techniques. Limnology and Oceanography-Methods, 10: 496-515.

Chen, M., Dei, R.C.H., Wang, W.-X. and Guo, L., 2003. Marine diatom uptake of iron bound with natural colloids of different origins. Marine Chemistry, 81(3-4): 177-189.

Chen, M. and Wang, W.X., 2001. Bioavailability of natural colloid-bound iron to marine plankton: Influences of colloidal size and aging. Limnology & Oceanography, 46(8): 1956-1967.

Chever, F. et al., 2010. Physical speciation of iron in the Atlantic sector of the Southern Ocean along a transect from the subtropical domain to the Weddell Sea Gyre. Journal of Geophysical Research, 115(C10): C10059.

Conway, T.M. and John, S.G., 2014. Quantification of sources of dissolved iron to the North Atlantic Ocean. Nature, 511: 212-215.

Croot, P. and Johansson, M., 2000. Determination of Iron Speciation by Cathodic Stripping Voltammetry in Seawater Using the Competing Ligand 2-(2-Thiazolylazo)-p-cresol (TAC). Electroanalysis, 12(8): 565-576.

Croot, P.L., Streu, P. and Baker, A.R., 2004. Short residence time for iron in surface seawater impacted by atmospheric dry deposition from Saharan dust events. Geophysical Research Letters, 31(23): L23S08.

Cullen, J.T., Bergquist, B.A. and Moffett, J.W., 2006. Thermodynamic characterization of the partitioning of iron between soluble and colloidal species in the Atlantic Ocean. Marine Chemistry, 98(2-4): 295-303.

Cutter, G.A. and Bruland, K.W., 2012. Rapid and noncontaminating sampling system for trace elements in a global ocean surveys. Limnology & Oceanography: Methods, 10: 425-436.

Draxler, R.R. and Rolph, G.D., 2014. HYSPLIT (HYbrid Single-Particle Lagrangian Integrated Trajectory) Model access via NOAA ARL READY Website (http://ready.arl.noaa.gov/HYSPLIT.php), NOAA Air Resources Laboratory, Silver Spring, MD.

ACCEPTED MANUSCRIPT

Fitzsimmons, J.N. and Boyle, E.A., 2012. An intercalibration between the GEOTRACES GO-FLO and the MITESS/Vanes sampling systems for dissolved iron concentration analyses (and a closer look at adsorption effects). Limnology & Oceanography: Methods, 10: 437-450.

Fitzsimmons, J.N. and Boyle, E.A., 2014a. Assessment and comparison of Anopore and cross flow filtration methods for the determination of dissolved iron size fractionation into soluble and colloidal phases in seawater. Limnology & Oceanography: Methods, 12: 244-261.

Fitzsimmons, J.N. and Boyle, E.A., 2014b. Both soluble and colloidal iron phases control dissolved iron variability in the tropical North Atlantic Ocean. Geochimica et Cosmochimica Acta, 125: 539-550.

Fitzsimmons, J.N. et al., in press. Partitioning of dissolved iron and iron isotopes into soluble and colloidal phases along the GA03 GEOTRACES North Atlantic Transect. Deep-Sea Research II.

Gledhill, M. and Buck, K.N., 2012. The organic complexation of iron in the marine environment: a review. Frontiers in Microbiology, 3: 69.

Gledhill, M. and van den Berg, C.M.G., 1994. Determination of complexation of iron(III) with natural organic ligands in seawater using cathodic stripping voltammetry. Marine Chemistry, 47: 41-54.

Hassler, C.S., Alasonati, E., Mancuso Nichols, C.A. and Slaveykova, V.I., 2011a. Exopolysaccharides produced by bacteria isolated from the pelagic Southern Ocean: Role in Fe binding, chemical reactivity, and bioavailability. Marine Chemistry, 123: 88-98.

Hassler, C.S., Schoemann, V., Nichols, C.M., Butler, E.C.V. and Boyd, P.W., 2011b. Saccharides enhance iron bioavailability to Southern Ocean phytoplankton. Proceedings of the National Academy of Sciences, 108(3): 1076-1081.

Hatta, M. et al., in press. An overview of dissolved Fe and Mn distributions during hte 2010-2011 U.S. GEOTRACES North Atlantic cruises. Deep-Sea Research II.

Jickells, T.D. et al., 2005. Global iron connections between desert dust, ocean biogeochemistry, and climate. Science, 308(5718): 67-71.

Kogut, M.B. and Voelker, B.M., 2001. Strong copper-binding behavior of terrestrial humic substances in seawater. Environmental Science and Technology, 35(6): 1149-1156.

Kuma, K. and Matsunaga, K., 1995. Availability of colloidal ferric oxides to coastal marine phytoplankton. Marine Biology, 122(1): 1-11.

Laglera, L.M. and van den Berg, C.M.G., 2009. Evidence for geochemical control of iron by humic substances in seawater. Limnology & Oceanography, 54(2): 610-619.

Langdon, C. (Editor), 2010. Determination of Dissolved Oxygen in Seawater by Winkler Titration Using the Amperometric Technique. The GO-SHIP Repeat Hydrography Manual: A Collection of Expert Reports and Guidelines, IOCCP Report Number 14.

Lee, J.-M. et al., 2011. Analysis of trace metals (Cu, Cd, Pb, and Fe) in seawater using single batch Nitrilotriacetate resin extraction and isotope dilution inductively coupled plasma mass spectrometry. Analytica Chimica Acta, 686: 93-101.

Liu, X. and Millero, F.J., 2002. The solubility of iron in seawater. Marine Chemistry, 77: 43-54.

Mackey, D.J. and Zirino, A., 1994. Comments on trace metal speciation in seawater or do "onions" grow in the sea? Analytica Chimica Acta, 284: 635-647.

Mahowald, N. et al., 2005. Atmospheric global dust cycle and iron inputs to the ocean. Global Biogeochemical Cycles, 19: GB4025.

Mantoura, R.F.C. and Riley, J.P., 1975. The use of gel filtration in the study of metal binding by humic acids and related compounds. Analytica Chimica Acta, 78: 193-200.

Martin, J.H. et al., 1994. Testing the iron hypothesis in ecosystems of the equatorial Pacific Ocean. Nature, 371: 123-129.

Mawji, E. et al., 2011. Production of siderophore type chelates in Atlantic Ocean water enriched with different carbon and nitrogen sources. Marine Chemistry, 124: 90-99.

ACCEPTED MANUSCRIPT

Measures, C.I., Hatta, M., Fitzsimmons, J.N. and Morton, P.L., in press. Dissolved Al in the zonal N Atlantic section of the US GETORACES 2010/2011 cruises and the importance of hydrothermal inputs. Deep-Sea Research II.

Millero, F.J., 1998. Solubility of Fe(III) in seawater. Earth and Planetary Science Letters, 154: 323-329.

Moore, J.K., Doney, S.C., Glover, D.M. and Fung, I.Y., 2002. Iron cycling and nutrient-limitation patterns in surface waters of the World Ocean. Deep Sea Research Part II: Topical Studies in Oceanography, 49(1-3): 463-507.

Morel, F.M.M., Kustka, A.B. and Shaked, Y., 2008. The role of unchelated Fe in the iron nutrition of phytoplankton. Limnology & Oceanography, 53(1): 400-404.

Morel, F.M.M., Milligan, A.J. and Saito, M.A., 2003. Marine Bioinorganic Chemistry: The Role of Trace Metals in the Oceanic Cycles of Major Nutrients. In: K.K. Turekian and H.D. Holland (Editors), Treatise On Geochemistry. Elsevier Science Ltd., Cambridge, United Kingdom, pp. 113-143.

Nishioka, J. et al., 2003. Size-fractionated iron distributions and iron-limitation processes in the subarctic NW Pacific. Geophysical Research Letters, 30(14): 1730.

Nishioka, J., Takeda, S., Wong, C.S. and Johnson, W.K., 2001. Size-fractionated iron concentrations in the northeast Pacific Ocean: distribution of soluble and small colloidal iron. Marine Chemistry, 74(2-3): 157-179.

Reitmeyer, R., Powell, R.T., Landing, W.M. and Measures, C.I., 1996. Colloidal aluminum and iron in seawater: An intercomparison between various cross-flow ultrafiltration systems. Marine Chemistry, 55: 75-91.

Rich, H.W. and Morel, F.M.M., 1990. Availability of well-defined iron colloids to the marine diatom *Thalassiosira weissflogii*. Limnology & Oceanography, 35(3): 652-662.

Rue, E.L. and Bruland, K.W., 1995. Complexation of iron(III) by natural organic ligands in the Central North Pacific as determined by a new competitive ligand equilibration/adsorptive cathodic stripping voltammetric method. Marine Chemistry, 50(1-4): 117-138.

Ružić, I., 1982. Theoretical aspects of the direct titration of natural waters and its information yield for trace metal speciation. Analytica Chimica Acta, 140: 99-113.

Scatchard, G., 1949. The attractions of proteins for small molecules and ions. Annals of the New York Academy of Sciences, 51: 660-672.

Schlosser, C. and Croot, P.L., 2008. Application of cross-flow filtration for determining the solubility of iron species in open ocean seawater. Limnology and Oceanography: Methods, 6: 630-642.

Sedwick, P.N., Sholkovitz, E.R. and Church, T.M., 2007. Impact of anthropogenic combustion emissions on the fractional solubility of aerosol iron: Evidence from the Sargasso Sea. Geochemistry Geophysics Geosystems, 8: 21.

Shaked, Y., Kustka, A.B. and Morel, F.M.M., 2005. A general kinetic model for iron acquisition by eukaryotic phytoplankton. Limnology & Oceanography, 50(3): 872-882.

Shelley, R.U., Morton, P.L. and Landing, W., in review. Elemental composition of North Atlantic aerosols (US GEOTRACES). Deep-Sea Research II U.S. GEOTRACES North Atlantic Special Issue.

Sholkovitz, E.R., Sedwick, P.N. and Church, T.M., 2009. Influence of anthropogenic combustion emissions on the deposition of soluble aerosol iron to the ocean: Empirical estimates for island sites in the North Atlantic. Geochimica Et Cosmochimica Acta, 73(14): 3981-4003.

Sunda, W.G., 2012. Feedback interactions between trace metal nutrients and phytoplankton in the ocean. Frontiers in Microbiology, 3: 204.

Talley, L.D., Pickard, G.L., Emery, W.J. and Swift, J.H., 2011. Descriptive Physical Oceanography. Elsevier Ltd.

Thuróczy, C.E. et al., 2010. Speciation of Fe in the Eastern North Atlantic Ocean. Deep Sea Research Part I: Oceanographic Research Papers, 57(11): 1444-1453.

ACCEPTED MANUSCRIPT

Town, R.M. and van Leeuwen, H.P., 2005. Measuring marine iron (III) complexes by CLE-AdSV. Environmental Chemistry, 2(2): 80-84.

Ussher, S.J. et al., 2010. Distribution of size fractionated dissolved iron in the Canary Basin. Marine Environmental Research, 70(1): 46-55.

van den Berg, C.M.G., 1982. Determination of copper complexation with natural organic ligands in sea water by equilibrium with MnO_2: I. Theory. Analytica Chimica Acta, 11: 307-312.

van den Berg, C.M.G., 1995. Evidence for organic complexation of iron in seawater. Marine Chemistry, 50(1-4): 139-157.

Velasquez, I. et al., 2011. Detection of hydroxamate siderophores in coastal and sub-Antarctic waters off the South Eastern coast of New Zealand. Marine Chemistry, 126: 97-107.

von der Heyden, B.P., Roychoudhury, A.N., Mtshali, T.N., Tyliszczak, T. and Myneni, S.C.B., 2012. Chemically and Geographically Distinct Solid-Phase Iron Pools in the Southern Ocean. Science, 338(6111): 1199-1201.

Vraspir, J. and Butler, A., 2009. Chemistry of marine ligands and siderophores. Annual Review of Marine Science, 1: 43-63.

Wagener, T., Guieu, C., Losno, R., Bonnet, S. and Mahowald, N., 2008. Revisiting atmospheric dust export to the Southern Hemisphere ocean: Biogeochemical implications. Global Biogeochem. Cycles, 22(2): GB2006.

Wang, W.X. and Dei, R.C.H., 2003. Bioavailability of iron complexed with organic colloids to the cyanobacteria *Synechococcus* and *Trichodesmium*. Aquatic Microbial Ecology, 33: 247-259.

Wells, M.L., 2003. The level of iron enrichment required to initiate diatom blooms in HNLC waters. Marine Chemistry, 82(1-2): 101-114.

Wells, M.L. and Goldberg, E.D., 1992. Marine submicron particles. Marine Chemistry, 40: 5-18.

Wells, M.L., Zorkin, N.G. and Lewis, A.G., 1983. The role of colloid chemistry in providing a source of iron to phytoplankton. Journal of Marine Research, 41: 731-746.

Worthington, L.V., 1959. The 18 ° water in the Sargasso Sea. Deep-Sea Research, 5: 297-305.

Wu, J., Boyle, E.A., Sunda, W.G. and Wen, L., 2001. Soluble and colloidal iron in the oligotrophic North Atlantic and North Pacific. Science, 293: 847-849.

Wu, J. and Luther, G.W., 1995. Complexation of Fe(III) by natural organic ligands in the Northwest Atlantic Ocean by a competitive ligand equilibration method and a kinetic approach. Marine Chemistry, 50(1-4): 159-177.

ACCEPTED MANUSCRIPT

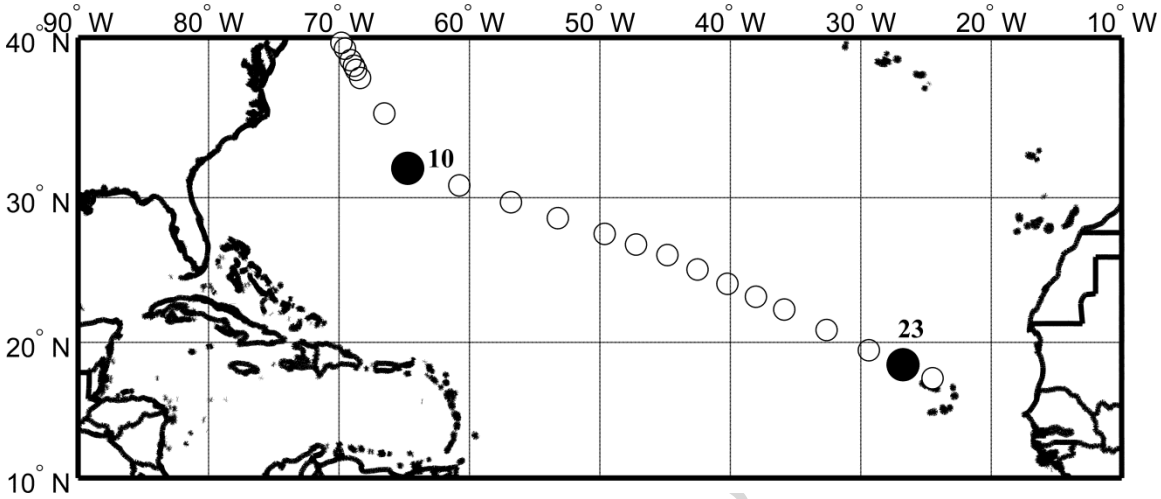

Figure 1

ACCEPTED MANU

ACCEPTED MANUSCRIPT

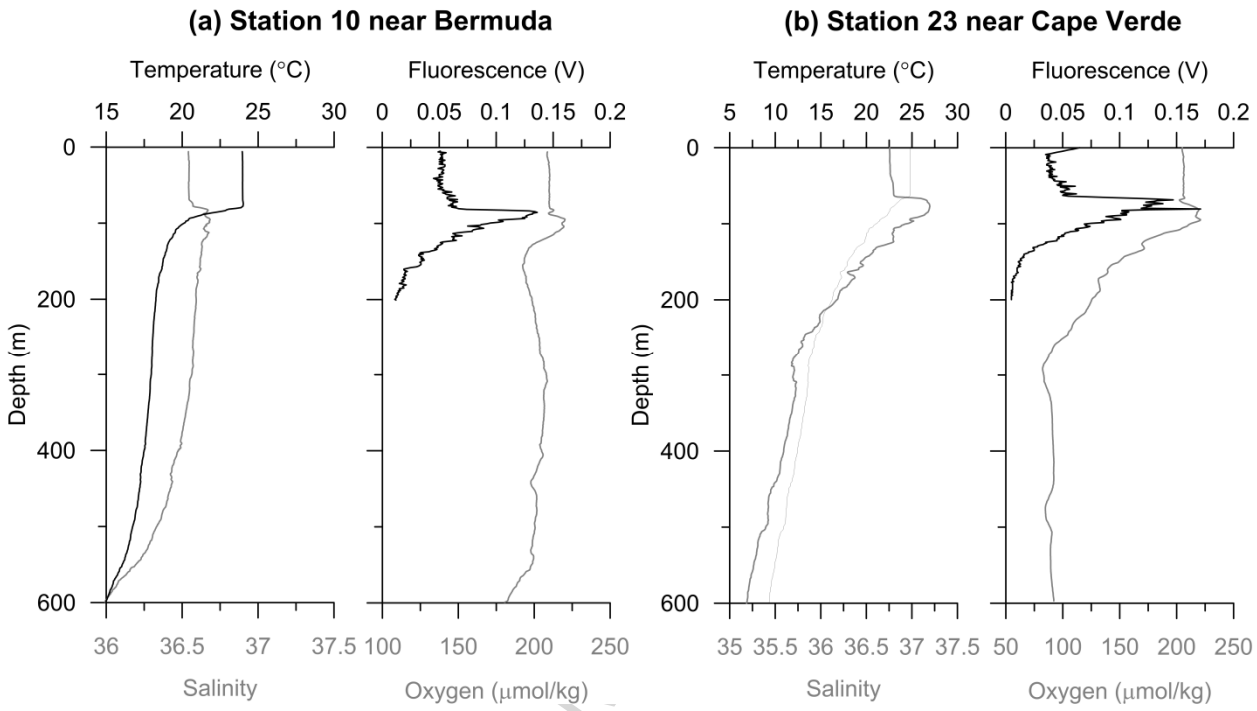

Figure 2

ACCEPTED MANUSCRIPT

ACCEPTED MANUSCRIPT

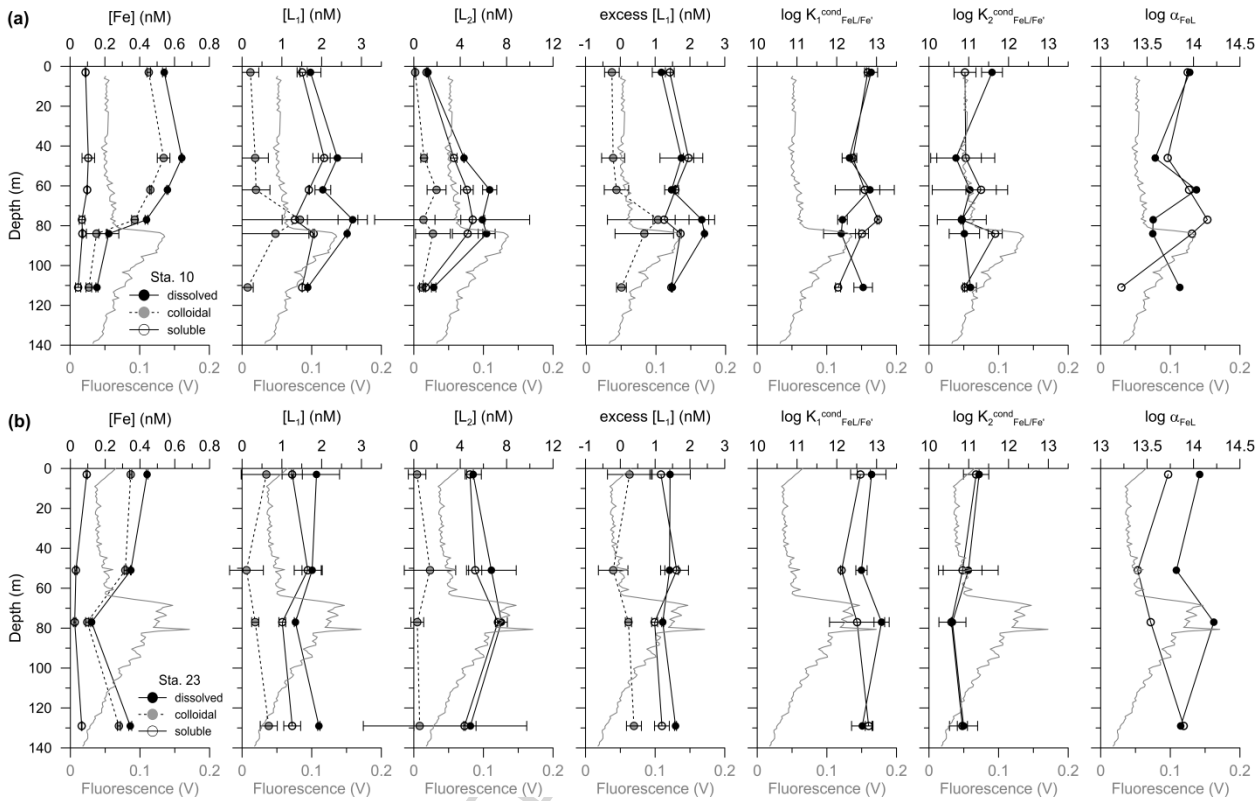

Figure 3

ACCEPTED

ACCEPTED MANUSCRIPT

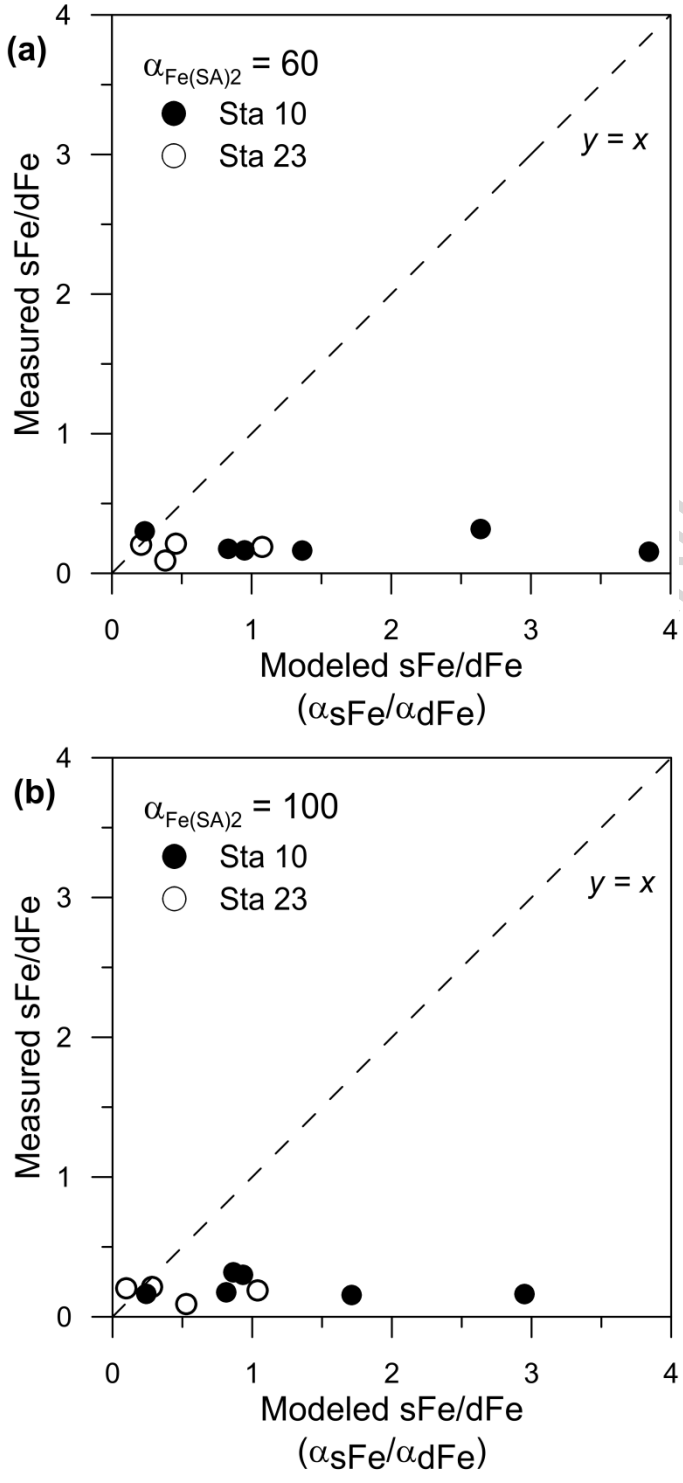

Figure 4

ACCEPTED MANUSCRIPT

Table 1

Station	Size Fraction	Depth (m)	[Fe] nmol L^{-1}	+/-	[L_1] nmol L^{-1}	+/-	logK_1	+/-	[L_2] nmol L^{-1}	+/-	logK_2	+/-
10	soluble	3	0.089	0.003	1.51	0.13	12.78	0.03	1.10	0.02	10.91	0.28
10	dissolved	3	0.541	0.010	1.72	0.26	12.87	0.16	1.22	0.04	11.59	0.26
10	soluble	46	0.105	0.036	2.07	0.15	12.41	0.05	3.45	0.27	10.93	0.73
10	dissolved	46	0.642	0.003	2.40	0.62	12.32	0.18	4.33	0.01	10.68	0.64
10	soluble	62	0.098	0.002	1.68	0.01	12.71	0.74	4.58	0.54	11.31	0.38
10	dissolved	62	0.559	0.004	2.03	0.20	12.84	0.25	6.54	0.61	11.03	0.95
10	soluble	77	0.068	0.016	1.33	0.32	13.04	0.03	5.08	1.03	10.83	0.62
10	dissolved	77	0.439	0.008	2.78	0.37	12.15	0.12	5.91	4.08	10.84	0.04
10	soluble	84	0.071	0.004	1.80	0.02	12.64	0.16	4.64	1.31	11.67	0.18
10	dissolved	84	0.222	0.058	2.64	0.00	12.12	0.45	6.28	0.73	10.89	0.38
10	soluble	111	0.046	0.015	1.51	0.00	12.04	0.06	1.03	0.00	10.91	0.05
10	dissolved	111	0.154	0.006	1.65	0.00	12.67	0.23	1.71	0.19	11.05	0.15
23	soluble	3	0.094	0.004	1.26	0.25	12.60	0.25	4.84	0.29	11.19	0.32
23	dissolved	3	0.441	0.005	1.87	0.58	12.88	0.36	5.12	0.70	11.26	0.00
23	soluble	51	0.032	0.007	1.65	0.34	12.12	0.03	5.29	0.57	10.85	0.49
23	dissolved	51	0.347	0.002	1.76	0.25	12.62	0.14	6.69	2.14	10.99	0.75
23	soluble	77	0.025	0.007	1.01	0.08	12.51	0.69	7.25	0.21	10.57	0.01
23	dissolved	77	0.122	0.005	1.34	0.03	13.13	0.19	7.55	0.51	10.59	0.34
23	soluble	129	0.065	0.002	1.26	0.21	12.80	0.08	4.37	0.07	10.84	0.13
23	dissolved	129	0.344	0.009	1.93	0.03	12.64	0.27	4.88	4.86	10.87	0.35

ACCEPTED MANUSCRIPT

Table 2

Station	Size Fraction	Depth (m)	[Fe] nmol L^{-1}	+/-	[L_1] nmol L^{-1}	+/-	logK_1	+/-	[L_2] nmol L^{-1}	+/-	logK_2	+/-
10	soluble	3	0.089	0.003	1.14	0.03	12.74	0.04	0.91	0.14	11.86	0.01
10	dissolved	3	0.541	0.010	1.47	0.05	13.44	0.18	5.60	0.16	11.27	0.02
10	soluble	46	0.105	0.036	2.27	0.04	13.08	0.03	1.09	0.22	11.82	0.26
10	dissolved	46	0.642	0.003	2.81	0.20	12.59	0.17	4.13	0.19	11.13	0.02
10	soluble	62	0.098	0.002	1.56	0.01	12.31	0.30	4.92	0.01	11.24	0.02
10	dissolved	62	0.559	0.004	2.34	0.02	12.29	0.00	6.38	0.09	11.29	0.00
10	soluble	77	0.068	0.016	1.59	0.04	12.75	0.05	4.89	0.02	11.21	0.23
10	dissolved	77	0.439	0.008	2.24	0.18	12.44	0.21	5.25	0.40	10.98	0.43
10	soluble	84	0.071	0.004	2.04	0.03	12.14	0.17	3.22	0.70	11.48	0.03
10	dissolved	84	0.222	0.058	3.04	0.16	12.08	0.17	4.61	0.21	11.28	0.03
10	soluble	111	0.046	0.015	1.98	0.01	12.49	0.16	1.52	0.14	11.49	0.06
10	dissolved	111	0.154	0.006	2.01	0.13	12.54	0.11	3.70	0.50	11.32	0.27
23	soluble	3	0.094	0.004	1.96	0.05	12.18	0.03	1.57	0.48	11.36	0.14
23	dissolved	3	0.441	0.005	2.00	0.05	12.83	0.04	3.02	0.03	11.56	0.02
23	soluble	51	0.032	0.007	1.10	0.10	12.70	0.10	5.52	0.20	10.81	0.09
23	dissolved	51	0.347	0.002	1.16	0.77	13.04	1.03	5.73	0.40	11.52	0.26
23	soluble	77	0.025	0.007	1.65	0.23	12.11	0.00	2.26	0.07	11.10	0.01
23	dissolved	77	0.122	0.005	1.96	0.08	13.21	0.20	2.52	0.05	11.80	0.09
23	soluble	129	0.065	0.002	2.89	0.05	12.18	0.01	3.46	0.30	10.93	0.42
23	dissolved	129	0.344	0.009	2.92	0.16	12.20	0.05	3.90	0.97	10.91	0.19

ACCEPTED MANUSCRIPT

Table 3

Station	Size Fraction	Depth	[Fe] nmol L^{-1}	$\alpha_{Fe(SA)2}$	$\log\alpha_{FeL}$	Modeled $\alpha_{sol}/\alpha_{diss}$	Measured Fe_{sol}/Fe_{diss}	α	logα	Modeled $\alpha_{sol}/\alpha_{diss}$	Measured Fe_{sol}/Fe_{diss}
10	soluble	3	0.089	60	13.94	0.95	0.16	100	13.81	0.24	0.16
10	dissolved	3	0.541	60	13.96			100	14.43		
10	soluble	46	0.105	60	13.72	1.36	0.16	100	14.43	2.95	0.16
10	dissolved	46	0.642	60	13.59			100	13.96		
10	soluble	62	0.098	60	13.95	0.83	0.18	100	13.58	0.81	0.18
10	dissolved	62	0.559	60	14.03			100	13.67		
10	soluble	77	0.068	60	14.15	3.84	0.16	100	13.97	1.71	0.16
10	dissolved	77	0.439	60	13.56			100	13.74		
10	soluble	84	0.071	60	13.98	2.64	0.32	100	13.57	0.86	0.32
10	dissolved	84	0.222	60	13.56			100	13.63		
10	soluble	111	0.046	60	13.22	0.23	0.30	100	13.81	0.93	0.30
10	dissolved	111	0.154	60	13.85			100	13.84		
23	soluble	3	0.094	60	13.73	0.46	0.21	100	13.51	0.28	0.21
23	dissolved	3	0.441	60	14.07			100	14.06		
23	soluble	51	0.032	60	13.40	0.38	0.09	100	13.76	0.53	0.09
23	dissolved	51	0.347	60	13.82			100	14.03		
23	soluble	77	0.025	60	13.54	0.21	0.20	100	13.38	0.10	0.20
23	dissolved	77	0.122	60	14.22			100	14.39		
23	soluble	129	0.065	60	13.89	1.08	0.19	100	13.66	1.04	0.19
23	dissolved	129	0.344	60	13.86			100	13.64		

ACCEPTED MANUSCRIPT

Table 4. Fe and Fe-binding ligand mass balance using cross flow filtration at 15 m depth at Station ALOHA in the Pacific Ocean.

Sample	**[Fe] nM**	**+/-**	**$[L]_T$ nM**	**+/-**	**[eL] nM**	**+/-**
Measured permeate ("soluble"), <10 kDa	0.039	0.008	0.300	0.008	0.262	0.011
Measured retentate	0.153	0.002	0.552	0.072	0.399	0.072
Measured CFF feed ("dissolved), <0.2 µm	0.176	0.014	0.654	0.032	0.478	0.035
Calculated colloidal (Equations 1 and 2)	0.057	0.008	0.126	0.072	0.068	0.073
Calculated soluble+colloidal	0.096	0.012	0.426	0.072	0.330	0.073
% Recovery	**54.5%**	*27%*	**65.1%**	*27%*	**69.1%**	*34%*

ACCEPTED MANUSCRIPT

ACCEPTED MANUSCRIPT

Table 5. Mass balance-calculated colloidal ligand characteristics (at $\alpha_{Fe(SA)_2}$ = 60) and the additional "kinetically-inhibited" colloidal L_2 concentrations required to explain the observed dFe size partitioning at equilibrium.

Sta.	Depth (m)	[cFe] nM	+/-	[Coll L_1] nM	+/-	Coll logK_1	[Coll L_2] nM	+/-	Coll logK_2	Additional [Coll L_2] nM
10	3	0.452	0.010	0.21	0.29	13.22	0.12	0.05	12.50	13.81
10	46	0.537	0.036	0.33	0.63	--	0.88	0.27	--	--
10	62	0.461	0.005	0.35	0.20	13.19	1.96	0.81	--	--
10	77	0.371	0.018	1.46	0.49	--	0.83	4.21	10.89	59.57
10	84	0.152	0.058	0.84	0.02	--	1.65	1.50	--	--
10	111	0.108	0.016	0.14	0.00	13.63	0.68	0.19	11.20	-0.33
23	3	0.347	0.006	0.61	0.63	13.17	0.28	0.76	11.83	1.63
23	51	0.316	0.007	0.11	0.42	13.67	1.40	2.22	11.31	4.72
23	77	0.097	0.009	0.33	0.09	13.65	0.30	0.55	10.96	0.03
23	129	0.279	0.009	0.67	0.21	11.85	0.51	4.86	11.07	7.63

ACCEPTED MANUSCRIPT

ACCEPTED MANUSCRIPT

Highlights

- Aerosol-derived surface dissolved Fe is mostly colloidal (10 kDa - 0.2 µm)
- Fe ligands in same waters, in contrast, are mostly soluble sized (<10 kDa)
- This suggests colloidal Fe is inorganic or colloidal ligands are undetected

ACCEPTED MANUSCRIPT